Desalination and Water Treatment
www.deswater.com

doi: 10.5004/dwt.2017.20268

64 (2017) 72–80
February

Preparation and characterization of modified PVDF membrane induced by argon plasma with enhanced antifouling property

Azadeh Ghaee[a,*], Behrouz Sadatnia[b], Mohammad Khosravi[c], Zahra Mansourpour[c], Ali Ghadimi[d]

[a]*Department of Life Science Engineering, Faculty of New Sciences and Technologies, University of Tehran, P.O. Box 143951374, Tehran, Iran, Tel./Fax: +98 21 88497324; email: ghaee@ut.ac.ir*
[b]*Department of Biomaterials, Iran Polymer and Petrochemical Institute, P.O. Box 14975/112, Tehran, Iran, Tel./Fax: +98 21 44787000; email: b.sadatnia@ippi.ac.ir*
[c]*School of Chemical Engineering, College of Engineering, University of Tehran, P.O. Box 11155/4563, Tehran, Iran, Tel./Fax: +98 21 61112196; emails: Mohammadkhosravi@alumni.ut.ac.ir (M. Khosravi), Mansourp@ut.ac.ir (Z. Mansourpour)*
[d]*Department of Petrochemicals Synthesis, Iran Polymer and Petrochemical Institute, P.O. Box 14975/112, Tehran, Iran, Tel./Fax: +98 21 44787000; email: a.ghadimi@ippi.ac.ir*

Received 2 May 2016; Accepted 15 October 2016

ABSTRACT

Poly(vinylidene fluoride) (PVDF) flat sheet membranes were fabricated by phase inversion method and modified with poly(acrylic acid) grafting induced by argon plasma. The effects of solvent type and coagulation bath temperature on membrane morphology and water flux were investigated. PVDF dopes were prepared by dissolving polymer powder in three different solvents: N,N-dimethylacetamide (DMAc), N,N-dimethylformamide (DMF) and 1-methyl-2-pyrrolidone (NMP). The differences in solubility parameters between the non-solvent, solvent and PVDF affected the phase inversion process, and the resulting morphology was observed by scanning electron microscopy (SEM). The results revealed that membranes fabricated using DMF and DMAc as solvents both exhibited short finger-like structures with spongy substrates. Also, the membrane morphology was altered toward a finger-like structure when the temperature of the coagulation bath was increased from 5°C to 55°C. The membranes with the highest water flux were modified with different concentrations of acrylic acid monomer and characterized by attenuated total reflection (ATR), SEM, atomic force microscopy (AFM), contact angle measurement and filtration tests. Results indicated that the membranes modified with higher concentrations of acrylic acid monomer displayed higher hydrophilicity and improved antifouling properties.

Keywords: Poly(vinylidene fluoride); Poly(acrylic acid); Argon plasma; Morphology; Antifouling

1. Introduction

Poly(vinylidene fluoride) (PVDF) is a semi-crystalline thermoplastic polymer that usually contains 59.4 wt% fluorine and 3 wt% hydrogen [1]. PVDF has several desirable specifications such as chemical resistance, thermal stability and high mechanical strength, which make it suitable candidate for membrane applications. PVDF is also a suitable material for use in water treatment applications due to its resistance to most acids, bases and oxidizing agents. Furthermore, PVDF can be easily dissolved in organic solvents due to its polarity, resulting from CH_2 and CF_2 groups in the polymer structure, which makes it possible for PVDF porous membranes to be fabricated using phase inversion techniques [1–5].

Phase inversion can be explained as a demixing process in which the initially homogeneous polymer solution is

* Corresponding author.

converted from a liquid phase to a solid state [6]. This conversion can take place in several ways, namely (a) thermally induced phase separation; (b) solvent controlled evaporation; (c) precipitation from the vapor phase and (d) immersion precipitation [6]. One of the most significant factors in phase inversion is the choice of solvent that has great impact on the morphology of the resulting membranes and finally attaining suitable membrane performance [7]. Among the solvents introduced for PVDF, N,N-dimethylacetamide (DMAc), N,N-dimethylformamide (DMF), 1-methyl-2-pyrrolidone (NMP) and dimethyl sulfoxide (DMSO) are considered strong solvents with high boiling points, while acetone and tetrahydrofuran (THF) are weaker solvents with low boiling points [8–10]. Yeow et al. [7] indicated that different solvents can have a great impact on the final membrane structure. They found that symmetrical cross-sectional membrane structure could be produced by using triethyl phosphate (TEP) as weak solvent, and water as the coagulation bath in spite of asymmetric morphology of membranes fabricated from dopes containing strong power solvents such as DMAc, NMP and DMF. Li et al. [11] produced four different PVDF membrane structures using four mixed solvents (trimethyl phosphate [TMP]–DMAc, TEP–DMAc, tricresyl phosphate–DMAc and tri-*n*-butyl phosphate–DMAc). The results of these experiments showed that strong solvents, such as TMP–DMAc and TEP–DMAc, resulted in higher precipitation rates and thus higher membrane water flux. Munari et al. [8] used DMF and NMP as solvents with high boiling temperatures in the presence or absence of either acetone or THF, as secondary solvents with low boiling temperatures. They concluded that evaporation time before immersion has no effect on the morphology and characteristics of the membranes prepared from solutions containing high boiling point solvents; however, it significantly affects the membrane characteristics when using low boiling point cosolvents [8].

Another factor that has considerable effect on the morphology of membranes prepared by phase inversion process is the temperature of the coagulation bath [7]. Cheng [12] has evaluated the effect of coagulation bath temperature on the morphology and crystalline structure of PVDF membranes prepared from PVDF/DMF/1-octanol and PVDF/DMF/water systems. Various temperatures between 25°C and 65°C were employed in the coagulation bath during membrane formation. Since crystallization occurred earlier than liquid–liquid demixing at 25°C, the final membranes were symmetrical in structure and contained identical PVDF spherical crystals [12]. On the other hand, asymmetric membranes featuring dense skin layers and cellular structures were formed at higher temperatures [12]. In another study, Wang et al. [13] studied the effect of coagulation bath temperature on the crystallinity of the resulting membranes. They observed that membranes prepared in a coagulation bath at 15°C had higher crystallinity than those formed at 60°C. They also found that membranes prepared at 60°C showed only the α-type crystal structure, while at 15°C the membranes contained a combination of both α- and β-type crystal structures [13].

After obtaining the appropriate structure, physical and chemical properties of membranes should be optimized for certain application. In spite of the broad advantages and applications of PVDF membranes, their hydrophobicity can pose a disadvantage in some applications. With regard to water treatment processes, the hydrophobicity of PVDF membranes is a drawback. This characteristic leads to membrane fouling by absorption of dissolved organic solutes and proteins on the membrane surface. In efforts to overcome this issue, various methods of membrane modification to increase hydrophilicity and reduce precipitation have shown promise. One technique to improve PVDF hydrophilicity is blending with different hydrophilic polymers like poly(vinylpyrrolidone) (PVP), poly(vinyl alcohol) (PVA) and poly(ethylene glycol) (PEG), although this modification can also alter the mechanical strength of the resulting membrane in comparison with pristine PVDF membranes [14,15]. Another way of increasing membrane hydrophilicity and improving its performance is the addition of inorganic nanoparticles (TiO_2, SiO_2, Al_2O_3, carbon nanotubes, graphene oxide) to the polymer dope. The challenge with this method is nanoparticle agglomeration in the casting solution, which influences the membrane's mechanical properties, morphology and performance [14,15]. Surface treatment of PVDF membranes through physical or chemical modifications is also an effective method for improving membrane hydrophilicity. In physical modification, membranes are immersed in hydrophilic polymer (PVA and chitosan) or active monomer solutions (acrylic acid [AA], 2-hydroxyethyl methacrylate or poly(ethylene glycol diacrylate)), and a thin hydrophilic layer is deposited or coated on the membrane surface [14,15]. Rahimpour et al. [16] used UV irradiation in order to deposit AA on PVDF membranes to improve its hydrophilicity, but resistance of PVDF to UV light resulted in inefficient surface activation [15]. PVDF membranes are usually activated by strong alkali or plasma treatment firstly to generate active groups [15]. To best of our knowledge, poly(acrylic acid) (PAA) grafting induced by argon plasma on PVDF membrane has not been reported in the literatures.

In this study, the morphology and chemical structure of PVDF membranes prepared using three different solvents including DMAc, DMF and NMP were investigated. Moreover, the effect of changes in coagulation bath temperature from 5°C to 55°C on the morphology of the membranes was studied. Afterward, the best membrane was selected as a suitable sublayer for PAA grafting by consideration of their morphology and water flux. The membrane surface was activated using argon plasma and immersed in different AA solutions. The resulting membranes were characterized by ATR, SEM, AFM, contact angle measurement and fouling experiments.

2. Experimental

2.1. Materials

Commercial PVDF polymer powders (Kynar 740) were supplied by Arkema, Philadelphia, USA. DAMc, NMP, DMF, AA and ammonium iron (II) sulfate were purchased from Merck, Germany, and used without further purification. In all cases, distilled water was used as the coagulation bath medium.

2.2. Fabrication of PVDF flat sheet membranes

PVDF polymer was dried at 50°C in a vacuum oven for 24 h to remove the moisture content. Dope solutions containing 20 wt% of polymer in various solvents (DMAc, DMF and NMP) were prepared through homogeneous stirring of the

mixture at 50°C for 24 h. Then, the dopes were degassed for 90 min in an ultrasonic bath (40°C) and stored at room temperature for 24 h before casting. Polymer solutions were cast as a thin film onto a glass plate at room temperature (25°C) and 60% ± 5% relative humidity with a 200-μm gap casting knife. The films were then immersed into a water bath at 25°C after 10 s evaporation time. In order to investigate the effect of coagulation bath temperature on the membrane morphology, polymer solutions with NMP solvent were cast as mentioned and then immersed in a distilled water coagulation bath (5°C–55°C) for 30 min. The prepared flat sheet membranes were kept in distilled water for 2 d before characterization to ensure the complete removal of the residual solvent.

2.3. Formation of PAA/PVDF composite membrane

PAA was grafted by argon plasma-induced polymerization onto the PVDF membranes that displayed an appropriate morphology and the highest water flux. Argon plasma modification can be explained as follows [17]: (1) During argon plasma treatment of a polymer, energy transfers from the plasma species to the polymer surface causing cleavage of certain chemical bonds and formation of free radicals. (2) After treatment, atmospheric oxygen reacts with free radicals, and functionalization occurs. (3) Peroxy radicals may react with small polymer fractions (P′). In hydrogenated systems, (4) chain peroxidation occurs and the POO$^{\bullet}$ radical can abstract a hydrogen atom from the polymer chain to form POOH, leading to the formation of another P$^{\bullet}$ radical that can further react with oxygen. Mohr's salt was used to suppress homopolymerization due to the fact that P′O$^{\bullet}$ radicals can initiate homopolymerization. The effect of Mohr's salt is to convert (5) the diperoxides POOP′ to P′O^{-} and (6) PO$^{\bullet}$ and $PO_2^{\bullet}$ to PO$^{\bullet}$ and O. In these procedures, (7) the homopolymer initiating species is $^{\bullet}$OH that is converted to OH^{-} by Fe^{2+} [18–20].

$$P \rightarrow P^{\bullet} \tag{1}$$

$$P^{\bullet} \xrightarrow{O_2} PO_2^{\bullet} \tag{2}$$

$$PO_2^{\bullet} + P' \rightarrow PO_2P' \tag{3}$$

$$PO_2^{\bullet} + PH \rightarrow POOH + P^{\bullet} \tag{4}$$

$$PO_2P' + Fe^{2+} \rightarrow PO^{\bullet} + P'O^{-} + Fe^{3+} \tag{5}$$

$$PO_2^{\bullet} + Fe^{2+} \rightarrow PO^{\bullet} + O^{-} + Fe^{3+} \tag{6}$$

$$^{\bullet}OH + Fe^{2+} \rightarrow OH^{-} + Fe^{3+} \tag{7}$$

Surface grafting of AA was performed by exposing the membranes to argon plasma (50 W, argon at 0.4 torr) for 1 min and then to air in order to allow peroxide formation on the membrane surface. Then the samples were immersed in aqueous AA solutions (30, 50 and 70 wt%) containing 0.0015 M ammonium iron(II) sulfate at 80°C for 5 h. Finally, the samples were washed to remove ungrafted AA monomers. The grafting degree was obtained by the following equation:

$$\text{Grafting degree}(\%) = \frac{W_g - W_0}{W_0} \tag{8}$$

where W_g and W_0 are membranes weights after and before grafting, respectively.

2.4. Characterization

2.4.1. ATR/FTIR analysis

The infrared (IR) spectra of the PVDF membranes with different solvents and coagulation bath temperatures and also composite membrane (PAA/PVDF) were recorded by fourier transform infrared (FTIR) analysis (Bruker, Germany) to study existing functional groups in the samples surfaces over the range of 600–4,000 cm^{-1}.

2.4.2. Scanning electron microscopy (SEM)

The morphology of the fabricated membranes was examined using SEM analysis. The membrane samples were immersed in liquid nitrogen and broken carefully. The samples were dried in a vacuum oven and sputtered with gold prior to SEM analysis. The SEM micrographs of sublayer cross sections and composite membranes were taken at various magnifications.

2.4.3. Pore size and porosity

Membrane porosity, ε (%), was determined by liquid displacement method by immersing the sublayers in 2-ethylhexanol overnight and weighing before and after alcohol absorption. It should be noted that the use of the alcohol in this test is related to its high persistence and permeability in PVDF membrane, because of its high boiling point of 180°C–188°C in the environment. The overall porosity was determined based on Eq. (9):

$$\varepsilon = \frac{\frac{m_n}{\rho_n}}{\frac{m_p}{\rho_p} + \frac{m_n}{\rho_n}} \tag{9}$$

where m_n, ρ_n, m_p and ρ_p are weight of absorbed 2-ethylhexanol (g), 2-ethylhexanol density (0.83 g/cm^3), weight of the dried membrane (g) and PVDF density (78.1 g/cm^3), respectively. Weight of the absorbed 2-ethylhexanol is measured by the difference of the wet and dry membranes.

The average pore radius (r_m) of the substrate membrane was calculated based on the pure water volume flux (J_W) and porosity (ε), using the Guerout–Elford–Ferry equation [21]:

$$r_m = \sqrt{\frac{(2.9 - 1.75\varepsilon) \times 8\eta t J_w}{\varepsilon A \Delta P}} \tag{10}$$

where η represents water viscosity (8.9×10^{-4} Pa s), ε membrane porosity (%), A effective membrane area (m^2), t the membrane thickness (m) and ΔP is the operating pressure (0.1 MPa). It should be mentioned that the unit of pure water volume flux, J_w, is m^3/s.

2.4.4. Membrane filtration experiments

A dead-end filtration system with N_2 cylinder connection (effective area of 28.26 cm^2 at 3 bar and 25°C) was used to determine water flux of sublayers and bovine serum albumin (BSA) rejection of composite membranes. First, the pure water experiment was done for 30 min, and water flux values were measured by weighing the permeate solution (J_1); then, the BSA solution (0.5 mg/ml) was used as feed and the flux (J_P), and protein concentration was calculated in the permeate solution. The BSA rejection was obtained using the following equation:

$$\text{BSA Rejection}(\%) = \left(1 - \frac{C_P}{C_F}\right) \times 100 \tag{11}$$

where C_P and C_F are BSA concentrations in the permeate and feed, respectively, measured using the standard Bradford method.

Finally, membranes were washed with distilled water, and their water flux (J_2) values were obtained. Flux recovery and total flux loss were calculated by the following equations [16]:

$$\text{Flux Recovery}(\text{FR})(\%) = \frac{J_2}{J_1} \times 100 \tag{12}$$

$$\text{Total flux loss} = \frac{J_1 - J_P}{J_1} \tag{13}$$

2.4.5. Atomic force microscopy

Surface roughness plays an important role in membrane wettability and antifouling properties. Top surface topography of the composite membranes was characterized using AFM (Dualscope/Rasterscope C26, DME, Denmark) in non-contact mode. The average roughness over the surface can be measured by AFM. Average surface roughness (R_a) and root mean square roughness (R_{rms}) data indicate significant deviations in texture characteristics [22]. R_a is the average roughness evaluated over the complete surface and defined as:

$$R_a = \iint_a \left|Z(x,y)\right| \cdot dx \cdot dy \tag{14}$$

where Z is the height function of the area.

R_q is the root mean square (rms) roughness expressed as follows:

$$R_q = \sqrt{\iint_a \left|Z(x,y)\right|^2 \cdot dx \cdot dy} \tag{15}$$

2.4.6. Contact angle

The hydrophilic character of the composite membranes was assayed using a water contact angle analyzer (Contact Angle Measurement System G10, KRUSS). A droplet of distilled water was mounted on the surface of each sample, and the average of three measurements at different points on the membrane was reported.

3. Results and discussion

3.1. Characterization of sublayers

3.1.1. Effect of solvent type on membrane morphology

Solvent type has a strong influence on the final properties and performance of the resulting membrane. Since the solvent type regulates the extent of polymer dissolution, a homogeneous or aggregated polymer solution can be formed based on the type of solvent used. With this in mind, a solution facilitating high polymer chain mobility can be achieved, as this property is controlled by both polymer–solvent and polymer–polymer interactions. The final morphology of fabricated membranes is largely dictated by physical factors including the solubility parameters of both the solvent/non-solvent and polymer/solvent systems. Hansen's three-dimensional solubility parameter (δ_t), which consists of a polar component (δ_p), a dispersion force component (δ_d), and a hydrogen bonding component (δ_h), can be used to analyze the relative affinity of a polymer/solvent/non-solvent system [23]. Since materials with similar (δ_t) values are likely to be miscible, the interaction between a polymer and solvent ($\Delta\delta_{ps}$) and interaction between a solvent and a non-solvent ($\Delta\delta_{sn}$) defined in the Eq. 16 can be used to examine the relative affinity of PVDF with NMP, DMAc and DMF [1,23–25]:

$$\Delta\delta_{ij} = [(\delta_{pi} - \delta_{pj})^2 + (\delta_{di} - \delta_{dj})^2 + (\delta_{hi} - \delta_{hj})^2]^{1/2} \tag{16}$$

where i and j denote the polymer and solvent or solvent and non-solvent, respectively. Table 1 lists the solubility parameters of PVDF, NMP, DMF and DMAc [23].

Table 1
Solubility parameters $(MPa)^{1/2}$ of PVDF, NMP, DMF, DMAc and water [23]

Chemicals	δ_d	δ_p	δ_h	Molar volume	δ_t[a]	$\Delta\delta_{ps}$	$\Delta\delta_{sn}$
PVDF	17.0	12.1	10.2	–	23.22	–	–
DMAc	16.8	11.5	10.2	92.5	22.77	0.632	32.48
NMP	18.0	12.3	7.2	96.5	22.95	3.168	35.38
DMF	17.4	13.7	11.3	77.0	24.86	1.982	31.14
Water	15.5	16.0	42.3	18.0	47.80	–	–

[a]The data is calculated from the repeating unit of the polymer $\delta_t = \sqrt{\delta_d{}^2 + \delta_p{}^2 + \delta_h{}^2}$.

Large difference in solubility parameters between the solvent and non-solvent ($\Delta\delta_{sn}$) facilitates diffusion of the non-solvent into the polymer film, leading to an increase in the exchange rate between solvent in the polymer film and the non-solvent in the coagulation bath. Immediate demixing caused by large differences in solubility is often associated with the formation of finger-like pores in the structure, whereas slower demixing results in the formation of a more sponge-like structure [23–25].

The phase separation behavior of PVDF as a semi-crystalline polymer is more complex than other amorphous polymers such as polysulfone and polyethersulfone [25]. In order to study the morphology of fabricated membranes in this study, three dope solutions were prepared using either DMAc (M_{DMAc}), DMF (M_{DMF}) or NMP (M_{NMP}) with equal PVDF concentration (20 wt%). The ATR spectra of fabricated membranes are shown in Fig. 1. For pristine PVDF membrane, the absorption bands at 875 and 1,400 cm^{-1} are associated with C–F vibration, and the peak at 1,178 cm^{-1} is attributed to the symmetrical stretching of $–CF_2$ groups [26]. On the other hand, the peak at 763 cm^{-1} can be assigned to in-plane bending in α phase, and the peaks at 840 and 1,069 cm^{-1} are due to stretching in β phase [26]. The fraction of β phase can be calculated based on the absorption bands of α phase (A_α) and β phase (A_β) as follows [27]:

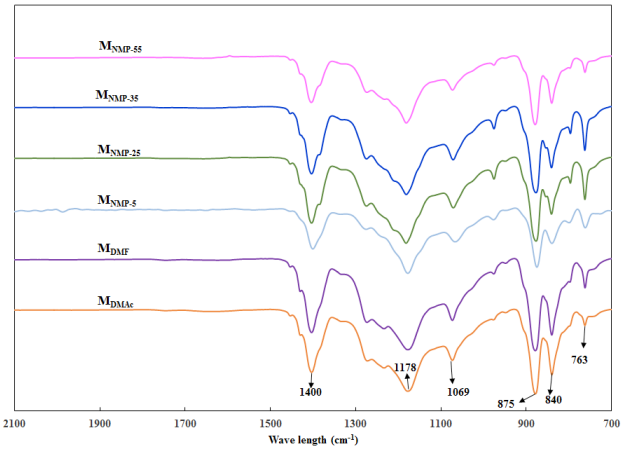

Fig. 1. ATR spectra of fabricated membranes with different solvents: DMAc, DMF in 25°C coagulation bath and NMP in 5°C, 25°C, 35°C and 55°C coagulation bath.

$$F(\beta) = \frac{A_\beta}{(1.26A_\alpha + A_\beta)} \quad (17)$$

PVDF chains are crystallized predominantly in β phase. As shown in Table 2, the $F(\beta)$ for $M_{NMP\text{-}25}$ is higher than for M_{DMAc} and M_{DMF} because of high $\Delta\delta_{sn}$ leading to fast solvent–non-solvent exchange and causes increase in polymer concentration near the interface of membrane and non-solvent. This increase in polymer concentration results in the formation of β phase in the top surface layers [27].

The SEM images of these membranes are shown in Fig. 2. As observed in Fig. 2, irregular macrovoids can be observed beneath the skin layer when NMP is used as the solvent. This is indicative of rapid skin layer formation due to the highest amount of $\Delta\delta_{sn}$, which leaves insufficient time for the further exchange of solvent/non-solvent under the surface. Prevention of further solvent outflow from under the skin layer led to the formation of macrovoids, where the solvent remained as the non-solvent continued to enter. Furthermore, flat sheet membranes fabricated using DMF and DMAc as solvents both exhibited shorter finger-like structures with spongy substrates. These two typical structures indicate a slow solvent/non-solvent exchange rate in the immersion–precipitation process. The mean pore size and porosity of prepared membranes are presented in Table 2. The results of Table 2 indicate that membranes prepared from NMP have the highest porosity and larger pore size compared with those prepared from DMAc and DMF. This observation is consistent with SEM results.

Similar results reported by Bottino et al. [10] demonstrated that the mechanism of PVDF membrane formation was governed more so by the kinetic factor, i.e., the mutual solvent/non-solvent diffusivity, rather than their thermodynamic properties.

3.1.2. Effect of coagulation bath temperature

Precipitation temperature is another critical factor influencing the final morphology and crystallinity of PVDF membranes. High precipitation temperatures tend to cause the formation of finger-like structures, while lower temperatures lead to a more sponge-like morphology and/or particle formation (if crystallization occurs) in the sublayer of PVDF membranes.

Dope solutions containing PVDF (20 wt%) with NMP as solvent were used for fabrication of membranes through an immersion–precipitation method. The IR spectra of prepared

Table 2
Sublayers specification and water flux

Samples	Polymer weight percentage (%)	Solvent	Coagulation bath temperature (°C)	$F(\beta)$ (%)	Water flux ($kg/m^2.h$)	Porosity (%)	Mean pore size (nm)
M_{DMAc}	20	DMAc	25	25.09	4.51	59.27	14.97
M_{DMF}	20	DMF	25	21.41	5.28	52.36	15.72
$M_{NMP\text{-}5}$	20	NMP	5	38.93	6.19	55.11	14.66
$M_{NMP\text{-}25}$	20	NMP	25	37.41	8.35	60.7	15.81
$M_{NMP\text{-}35}$	20	NMP	35	35.75	9.32	62.32	16.35
$M_{NMP\text{-}55}$	20	NMP	55	33.47	10.76	72.68	17.26

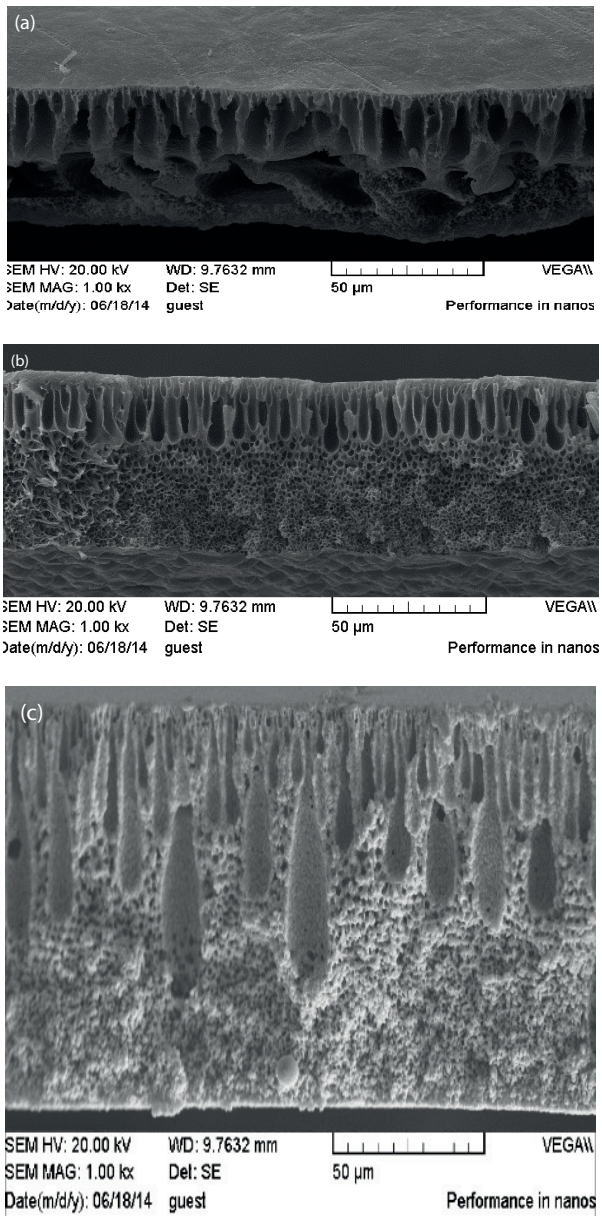

Fig. 2. SEM images of fabricated membranes with different solvents: (a) NMP, (b) DMAc and (c) DMF in 25°C coagulation bath.

membranes with different coagulation bath temperatures are shown in Fig. 1. The characteristic bands are the same as the membrane with different solvents (section 3.1.1). The amount of $F(\beta)$ enhanced with coagulation bath temperature reduction. This means that crystallization occurs faster in lower coagulation bath temperatures. Cheng [12] results confirmed this observation.

Fig. 3 shows the SEM images of these membranes, where it was found that an increase in the coagulation bath temperature had an influence on the coagulation rate of PVDF membrane. The morphology of the membranes in Figs. 3(a) and (b) is finger-like with larger macrovoids in $M_{NMP\text{-}55}$. Elevated coagulation bath temperatures enhanced the kinetics of the solvent efflux and water influx. Therefore, at high temperatures, crystallization can be suppressed long enough

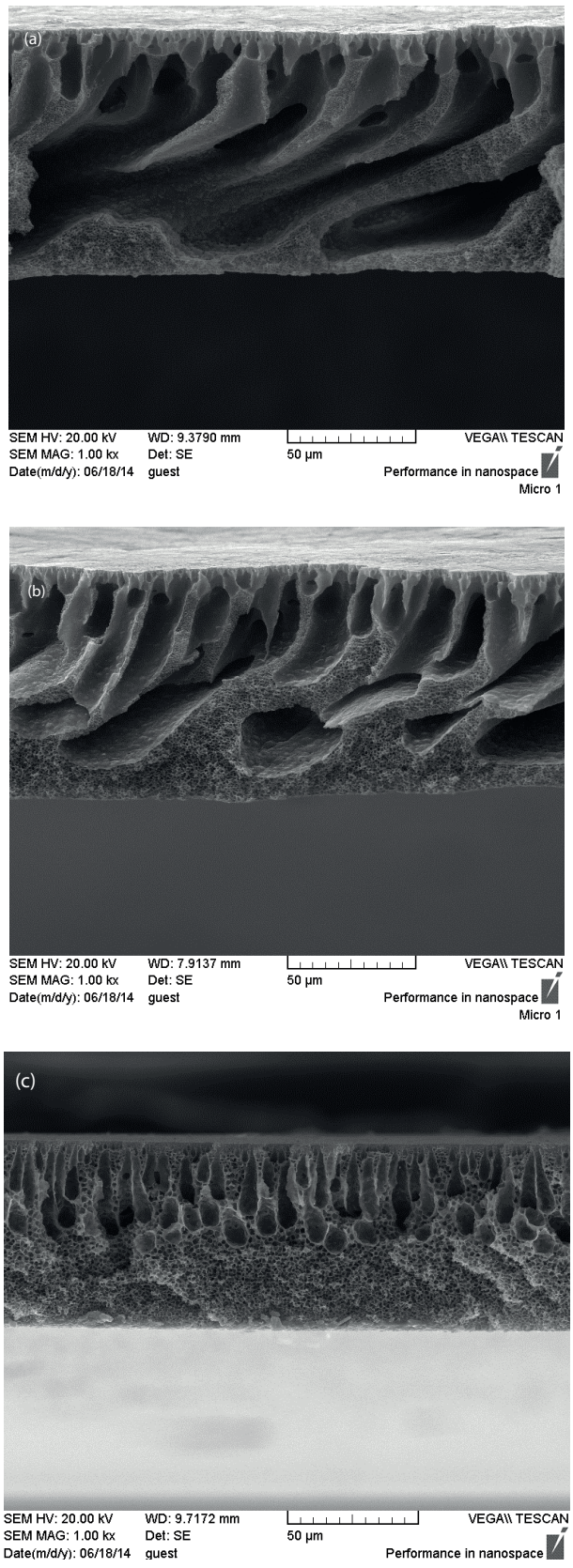

Fig. 3. SEM images of PVDF membranes were casted in 5°C–55°C coagulation bath temperature: (a) 55°C, (b) 35°C and (c) 5°C (solvent is NMP).

to allow thorough liquid–liquid demixing, which consequently pushes the membrane structure toward a finger-like morphology. On the other hand, gelation was induced at low temperature by the occurrence of crystallization first in the membrane formation sequence, and crystals were allowed to grow due to slow liquid–liquid demixing; thus, the membrane structure became more sponge-like as can be seen in Fig. 3(c) [12]. Furthermore, by increasing the coagulation bath temperature, membrane pore size and porosity are increased (Table 2).

Cheng [12] also studied the effect of coagulation bath temperatures on PVDF membrane morphology. In this study, a change in the coagulation bath temperature from 25°C to 65°C incited a corresponding change in membrane morphology from a symmetric structure composed of spherical crystallites to an asymmetric structure with a dense top layer accompanied by a cellular structure mixed with spherical particles. The former morphology could be described by the occurrence of crystallization-dominated precipitation, while the latter is attributed to liquid–liquid demixing. A similar conclusion was drawn by Wang et al. [13].

3.1.3. Membrane filtration experiments

The water fluxes of different sublayers, which were prepared using different solvents and coagulation bath temperatures, are reported in Table 2. The membrane prepared with NMP as solvent had the highest permeability in comparison with membranes prepared with DMAc and DMF, due to its channel-like structure (Fig. 2(a)). Also at the maximum coagulation bath temperature (55°C), the membrane water flux was the highest because of its channel-like structure (Fig. 3(a)) as opposed to the sponge-like structure of membranes prepared in lower coagulation bath temperatures, which was confirmed by SEM observation. Considering the morphology and water flux of the prepared membranes, $M_{NMP\text{-}55}$ was chosen as the best sublayer for composite membrane preparation.

3.2. Characterization of composite membranes

3.2.1. ATR/FTIR

ATR spectra of PVDF and PAA/PVDF composite membranes are shown in Fig. 4. Plasma-generated free radicals on membrane surface are then exposed to atmosphere resulting in peroxide formation, which initiates grafting from polymerization in the presence of unsaturated monomers [26]. All mentioned characteristic peaks (in section 3.1.1) of pristine PVDF membranes can be observed for PAA/PVDF composite membranes. Moreover, an absorption peak at 1,728 cm^{-1} [16–20,26,28], assigned to C=O bond stretching of the PAA carboxylic acid groups, can be observed, which confirms PAA formation.

3.2.2. SEM, grafting degree and contact angle

The SEM cross-sectional images of the PAA layer in the composite membranes are shown in Fig. 5. It can be observed that by increasing AA concentration in the grafting process, the top layer became thicker. Furthermore, the grafting degree and contact angle of prepared membranes with

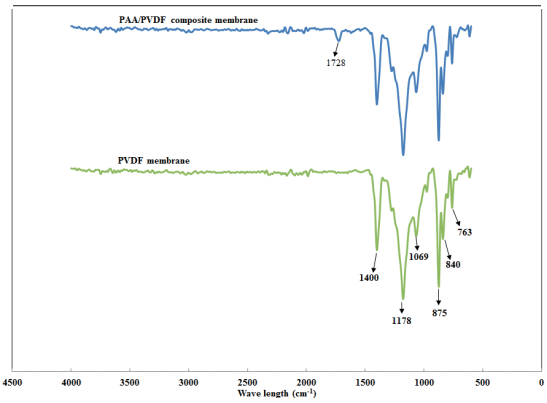

Fig. 4. ATR spectra of unmodified and modified membranes.

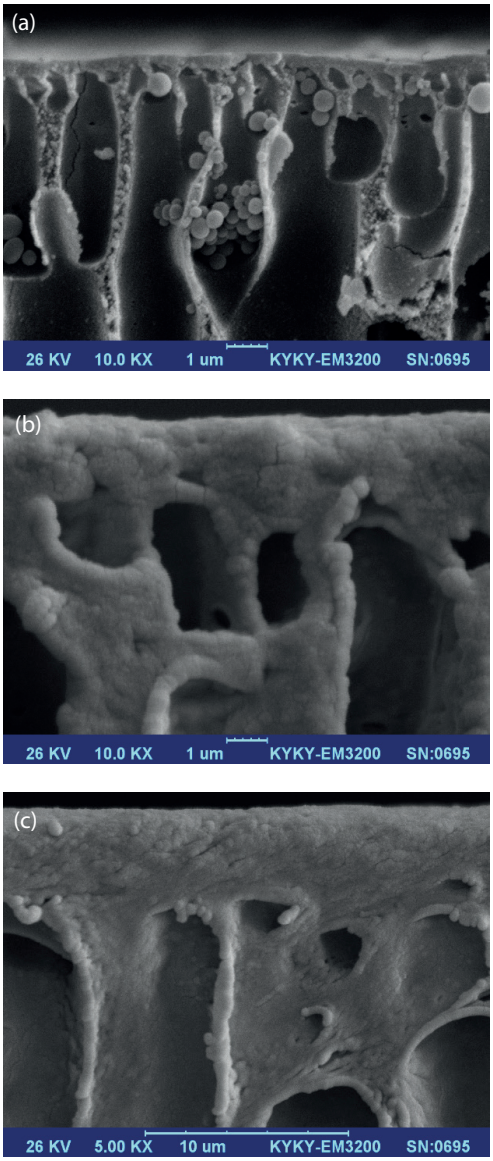

Fig. 5. SEM images of modified membranes with: (a) 10% acrylic acid solution, (b) 30% acrylic acid solution and (c) 70% acrylic acid solution.

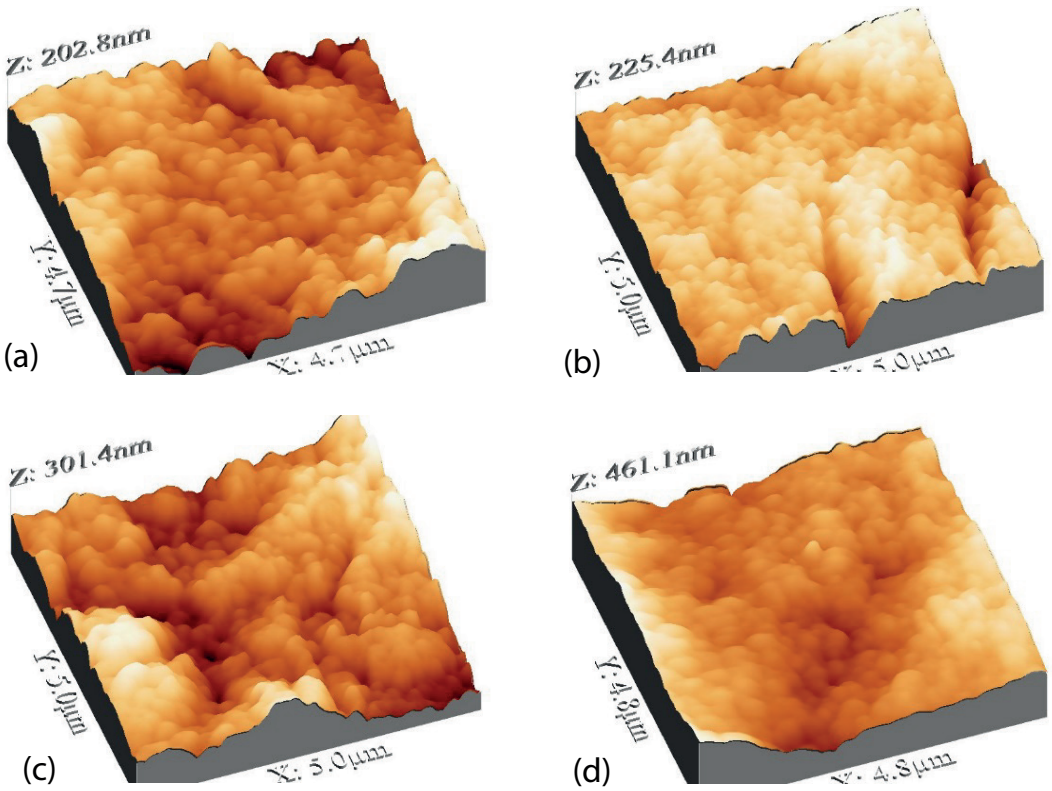

Fig. 6. Surface topography of: (a) pristine PVDF, (b) 10% acrylic acid solution, (c) 30% acrylic acid solution and (d) 70% acrylic acid solution.

different concentrations of AA are presented in Table 3. With increase in AA concentration, there was increase in the grafting degree, which is confirmed by SEM analysis. There is a logarithmic relationship between AA grafting to fluoropolymers and its concentration, which increased with monomer concentration increase [18]. Moreover, the contact angle of the prepared membranes was reduced due to the enrichment of PAA chains and remaining polar groups from plasma treatment [26] on the membrane surface.

Table 3
Unmodified and modified membranes' grafting degree, contact angle and roughness parameters

Samples	Grafting degree (%)	Contact angel (°)	R_a (nm)	R_q (nm)
Unmodified	–	88.2	20.24	26.49
Modified in 10% AA	1.8	81.5	25.09	32.74
Modified in 30% AA	4.3	72.3	29.6	41.25
Modified in 70% AA	8.5	58.4	34.8	49.13

3.2.3. Surface topography

Surface topography and roughness parameters are shown in Fig. 6 and Table 3. The average roughness of the membrane modified with 10% AA increased compared with pristine PVDF membrane. The highest R_a is for the membrane modified with 70% AA and has direct effect on contact angle results. Wenzel described the effect of roughness on surface wettability. He claimed that increase in surface roughness will result in enhancing the wettability caused by the chemical properties [29]. In other words, if the surface is hydrophilic chemically, surface hydrophilicity will rise by introducing roughness. The contact angle results confirmed the surface topography observations.

Table 4
Performance and antifouling properties of unmodified and modified membranes

Samples	Water flux (kg/m².h)	BSA rejection (%)	Flux recovery (%)	Total flux loss
Unmodified	10.76	91	57	0.89
Modified in 10% AA	8.42	94	59	0.82
Modified in 30% AA	6.14	95	62	0.76
Modified in 70% AA	4.89	98	69	0.69

3.2.4. Antifouling properties

The water flux and fouling experiment results of composite membranes are presented in Table 4. Membrane hydrophilicity has an important role in membrane fouling, and by increasing the hydrophilicity, the water adsorption on membrane surface and as a result water permeation increases for the membrane modified by 10% AA monomers. But, the water flux of the modified membranes decreased

with grafting degree enhancement due to thicker skin layer formation. Also, increasing the grafting degree caused BSA rejection improvement due to an increase in hydrophilicity, which hinders protein adsorption on the membrane surface and enhances the retention. Moreover, flux recovery was enhanced by grafting degree, indicating PAA grafting resulted in enhanced reversible fouling. Grafting PAA reduces adsorption of BSA on PVDF membrane by weakening the hydrophobic interaction between BSA and PVDF on membrane surface, and pollutants can be removed by washing easily.

4. Conclusion

Porous asymmetric PVDF membranes were prepared by phase inversion induced by a non-solvent. The final morphology of PVDF membranes after fabrication with three different solvents, including NMP, DMF and DMAc, was investigated. Experimental results revealed the distinctive influences of various solvents on the resulting membrane structure, indicating the main role of the solvent. Given large differences in the solubility parameters between the solvent and non-solvent ($\Delta\delta_{sn}$) led to an instantaneous demixing, which is normally accompanied by the formation of a finger-like structure. Effects of the coagulation bath temperature on membrane formation were investigated using SEM images. At lower temperatures, gelation was induced by crystallization, and crystals were able to grow due to slow liquid–liquid demixing, which ultimately resulted in the membrane structure adopting a more sponge-like morphology. After modifying the membrane surface with PAA, membrane water permeation and fouling declined, and BSA rejection capability was enhanced due to an increase in membrane hydrophilicity.

References

[1] J.E. Dohany, Fluorine-Containing Polymers, Poly(Vinylidene Fluoride), Kirk-Othmer Encyclopedia of Chemical Technology, John Wiley & sons, New York, 2000.

[2] K. Oshima, T. Evans-Strickfaden, A. Highsmith, E. Ades, The use of a microporous polyvinylidene fluoride (PVDF) membrane filter to separate contaminating viral particles from biologically important proteins, Biologicals, 24 (1996) 137–145.

[3] S.S. Madaeni, M.K. Yeganeh, Microfiltration of emulsified oil wastewater, J. Porous Mater., 10 (2003) 131–138.

[4] S.R. Chae, H. Yamamura, K. Ikeda, Y. Watanabe, Comparison of fouling characteristics of two different poly-vinylidene fluoride microfiltration membranes in a pilot-scale drinking water treatment system using pre-coagulation/sedimentation, sand filtration, and chlorination, Water Res., 42 (2008) 2029–2042.

[5] D. Wang, W. Teo, K. Li, Selective removal of trace H_2S from gas streams containing CO_2 using hollow fibre membrane modules/contractors, Sep. Purif. Technol., 35 (2004) 125–131.

[6] M. Mulder, Basic Principles of Membrane Technology, Springer, Netherlands, 1996.

[7] M. Yeow, Y. Liu, K. Li, Morphological study of poly(vinylidene fluoride) asymmetric membranes: effects of the solvent, additive, and dope temperature, J. Appl. Polym. Sci., 92 (2004) 1782–1789.

[8] S. Munari, A. Bottino, G. Capannelli, Casting and performance of polyvinylidene fluoride based membranes, J. Membr. Sci., 16 (1983) 181–193.

[9] T. Uragami, Y. Naito, M. Sugihara, Studies on synthesis and permeability of special polymer membranes, Polym. Bull., 4 (1981) 617–622.

[10] A. Bottino, G. Camera-Roda, G. Capannelli, S. Munari, The formation of microporous polyvinylidene difluoride membranes by phase separation, J. Membr. Sci., 57 (1991) 1–20.

[11] Q. Li, Z.L. Xu, L.Y. Yu, Effects of mixed solvents and PVDF types on performances of PVDF microporous membranes, J. Appl. Polym. Sci., 115 (2010) 2277–2287.

[12] L.P. Cheng, Effect of temperature on the formation of microporous PVDF membranes by precipitation from 1-octanol/DMF/PVDF and water/DMF/PVDF systems, Macromolecules, 32 (1999) 6668–6674.

[13] X. Wang, L. Zhang, D. Sun, Q. An, H. Chen, Formation mechanism and crystallization of poly(vinylidene fluoride) membrane via immersion precipitation method, Desalination, 236 (2009) 170–178.

[14] F. Liu, N.A. Hashim, Y. Liu, M.R. Moghareh Abed, K. Li, Progress in the production and modification of PVDF membranes, J. Membr. Sci., 375 (2011) 1–27.

[15] G.D. Kang, Y.M. Cao, Application and modification of poly(vinylidene fluoride) (PVDF) membranes, J. Membr. Sci., 463 (2014) 145–165.

[16] A. Rahimpour, S.S. Madaeni, S. Zereshki, Y. Mansourpanah, Preparation and characterization of modified nano-porous PVDF membrane with high antifouling property using UV photo-grafting, Appl. Surf. Sci., 255 (2009) 7455–7461.

[17] J. Chen, Y.C. Nao, J.S. Park, Grafting polymerization of acrylic acid onto preirradiated polypropylene fabric, Radiat. Phys. Chem., 52 (1998) 201–206.

[18] T.R. Dargaville, G.A. George, D.J.T. Hill, A.K. Whittaker, High energy radiation grafting of fluoropolymers, Prog. Polym. Sci., 28 (2003) 1355–1376.

[19] A. Bozzi, A. Chapiro, Synthesis of perm-selective membranes by grafting acrylic acid into air-irradiated Teflon-FEP films, Int. J. Radiat. Appl. Instrum. Part C, 32 (1988) 193–196.

[20] F. Liu, B.K. Zhu, Y.Y. Xu, Improving the hydrophilicity of poly(vinylidene fluoride) porous membranes by electron beam initiated surface grafting of AA/SSS binary monomers, Appl. Surf. Sci., 253 (2006) 2096–2101.

[21] E. Salimi, A. Ghaee, A.F. Ismail, Performance and antifouling enhancement of polyethersulfone hollow fiber membranes incorporated with highly hydrophilic hydroxyapatite nanoparticles, RSC Adv., 6 (2016) 44480–44488.

[22] A. Ghaee, M. Shariaty-Niassar, J. Barzin, T. Matsuura, Effects of chitosan membrane morphology on copper ion adsorption, Chem. Eng. J., 165 (2010) 46–55.

[23] J. Hirschinger, D. Schaefer, H.W. Spiess, A.J. Lovinger, Chain dynamics in the crystalline α-phase of poly(vinylidene fluoride) by two-dimensional exchange deuteron NMR, Macromolecules, 24 (1991) 2428–2433.

[24] W.M. Haynes, CRC Handbook of Chemistry and Physics, CRC Press, Boca Raton, 2014.

[25] I.M. Wienk, R. Boom, M. Beerlage, A. Bulte, C. Smolders, H. Strathmann, Recent advances in the formation of phase inversion membranes made from amorphous or semi-crystalline polymers, J. Membr. Sci., 113 (1996) 361–371.

[26] S.J. You, G.U. Semblante, S.C. Lu, R.A. Damodar, T.C. Wei, Evaluation of the antifouling and photocatalytic properties of poly(vinylidene fluoride) plasma-grafted poly(acrylic acid) membrane with self-assembled TiO_2, J. Hazard. Mater., 237–238 (2012) 10–19.

[27] M.M. Tao, F. Liu, B.R. Ma, L.X. Xue, Effect of solvent power on PVDF membrane polymorphism during phase inversion, Desalination, 316 (2013) 137–145.

[28] L. Ying, P. Wang, E.T. Kang, K.G. Ne, Synthesis and characterization of poly(acrylic acid)-*graft*-poly(vinylidene fluoride) copolymers and pH-sensitive membranes, Macromolecules, 35 (2002) 673–679.

[29] S. Tohidi, A. Ghaee, J. Barzin, Preparation and characterization of poly(lactic-co-glycolic acid)/chitosan electrospun membrane containing amoxicillin-loaded halloysite nanoclay, Polym. Adv. Technol., 27 (2016) 1020–1028. doi: 10.1002/pat.3764.